

# Comparing 3D Shape and Texture Descriptors Towards Tourette's Syndrome Prediction Using Pediatric Magnetic Resonance Imaging

Murilo Costa de Barros<sup>1</sup><sup>a</sup>, Kaue Tartarotti Nepomuceno Duarte<sup>2</sup><sup>b</sup>, Chia-Jui Hsu<sup>4</sup>,  
Wang-Tso Lee<sup>3</sup><sup>c</sup> and Marco Antonio Garcia de Carvalho<sup>1</sup><sup>d</sup>

<sup>1</sup>Computing Visual Laboratory, School of Technology - UNICAMP,

R. Paschoal Marmo, 1888 - Jd. Nova Itália, 13484-332 - Limeira, São Paulo, Brazil

<sup>2</sup>Vascular Imaging Laboratory, Calgary University, 2500 University Dr NW, Calgary, AB T2N 1N4, Canada

<sup>3</sup>Department of Pediatrics, National Taiwan University Hospital Hsinchu Branch, Hsinchu, 300001, Taiwan

<sup>4</sup>Department of Pediatrics, National Taiwan University Children's Hospital, Taiwan

**Keywords:** Tourette Syndrome, GLCM, Texture Feature, Shape Feature, Image Processing, Classification, Machine Learning, MRI.


**Abstract:** Tourette Syndrome (TS) is a neuropsychiatric disorder characterized by the presence of involuntary motor and vocal tics, with its etiology suggesting a strong and complex genetic basis. The detection of TS is mainly performed clinically, but brain imaging provides additional insights about anatomical structures. Interpreting brain patterns is challenging due to the complexity of the texture and shape of the anatomical regions. This study compares three-dimensional texture and shape features using Gray-Level Co-occurrence Matrix and Scale-Invariant Heat Kernel Signature. These features are analyzed in the context of TS classification (via Support Vector Machines), focusing on anatomical regions believed to be associated with TS. The evaluation is performed on structural Magnetic Resonance (MR) images of 68 individuals (34 TS patients and 34 healthy subjects). Results show that shape features achieve 92.6% accuracy in brain regions like the right thalamus and accumbens area, while texture features reach 73.5% accuracy in regions such as right putamen and left thalamus. Majority voting ensembles using shape features obtain 96% accuracy, with texture features achieving 79.4%. These findings highlight the influence of subcortical regions in the limbic system, consistent with existing literature on TS.


## 1 INTRODUCTION


Tourette Syndrome (TS) is a genetic condition with neuroanatomical and neurophysiological alterations, mainly characterized by motor and vocal manifestations commonly known as tics (Johnson et al., 2023). The development of TS typically occurs before the age of 18, with the first symptoms potentially emerging between the ages of 4 and 6 years. The tics can change, either by decreasing or increasing in intensity during the growth process. TS is known to affect approximately 1% of the world population and is more commonly diagnosed in male children (Jones et al., 2023). Tics can be classified into two categories: *simple*


*ple tics*, consisting of blinking, involuntary shoulder movement, neck and lip twitching, and in some cases, even coughing or grunting; and *complex tics*, which tend to be more drastic, such as self-injurious behavior or jumping (Cen et al., 2020). Diagnosing the syndrome is challenging due to the potential presence of other comorbidities, such as Attention Deficit Hyperactivity Disorder (ADHD), Obsessive-Compulsive Disorder (OCD), as well as the coexistence of anxiety, depression, and other psychiatric manifestations (Jones et al., 2023). (Figure 1)

TS is a complex topic of study due to changes in specific brain regions, such as caudate, thalamus, and certain cortical areas. However, these alterations are often difficult to identify solely through medical appointments. While current literature express the advantages of diagnosing TS via clinical data (Pringsheim et al., 2023), the increased use of medical imaging modalities, such as structural Magnetic Res-

<sup>a</sup> <https://orcid.org/0000-0003-2452-8128>

<sup>b</sup> <https://orcid.org/0000-0002-4074-3672>

<sup>c</sup> <https://orcid.org/0000-0003-3231-9764>

<sup>d</sup> <https://orcid.org/0000-0002-6303-5564>

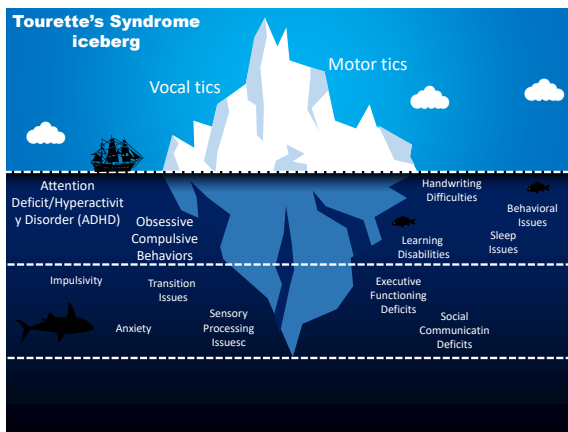


Figure 1: Tourette's Syndrome: What we can see VS what it can hide. Adapted from (Tourette.org, 2017).

onance (MR) images, is expected to provide beneficial outcomes since it can identify patterns in the brain that are hidden from human eyes. These patterns can be captured by feature descriptors, techniques that extract specific information from a given structure. Two prominent styles of feature extraction are either by texture (repetitive occurrence of intensity tone in a region) or by shape (complex boundaries that surround a certain region). However, there is no consensus on which feature extraction style is better, leaving the choice to the specific application.

In this work, we adopted a 3D Gray-Level Co-occurrence Matrix (GLCM) (Haralick et al., 1973) to extract texture features, whereas the 3D Scale-Invariant Heat Kernel Signature (SIHKS) (Kamara-jugadda and Pavani, 2022) has been used to extract shape features. A further processing step is often performed to interpret these features, which can serve as input to classify, for example, whether a child has TS. Machine Learning (ML) techniques are commonly used for this purpose, as they allow for unsupervised feature classification.

The main goal of this work is to classify TS patients by comparing texture and shape features obtained in MR images. The main contributions of this work are: (1) classifying TS patients using shape and texture features; (2) identifying brain regions that are more susceptible to TS; and (3) studying which feature extractor ensemble is efficient for classifying TS.

The remaining sections of this paper are organized as follows: the Section 2 outlines the existing work and identifies the research gaps; In Section 3, it is described our materials and proposed method; Section 4 provides our results, which are further discussed in Section 5; Finally, Section 6 provides a summary and conclusion of our work.

## 2 LITERATURE REVIEW

Adopting advanced computer methods to interpret TS poses challenges due to slight known changes in both texture and shape of anatomical regions. Most of work often focus on clinical information, which might not consider important unseen aspects of the subject's brain. However, such work that employs shape and texture features have been frequently used in other disorders (Betrouni et al., 2021).

Texture features have strong spatial characterization that allows distinguishing between healthy and symptomatic patients. In Silva (Silva et al., 2023), a technique that involves GLCM and Wavelet transforms is used to classify Alzheimer's Disease (AD) in three possible prodromal stages. They studied the implication of using distinct classifiers, such as Support Vector Machines (SVM) and Random Forests (RF), towards improving the accuracy of the models. They have shown that aligning texture and machine learning classification has the potential to unveil undiscovered brain patterns. Aside from AD, texture features have also been adopted in the context of Parkinson's Disease (PD) (Betrouni et al., 2021), where the authors classified two symptomatic stages (early and late PD) against healthy normal. First- and second-order texture features have shown that regions like putamen, thalamus, and caudate had shown significant results. Shifting the attention to TS, 3D texture patterns have been employed by (Barros et al., 2022) in the context of identifying the statistically relevant anatomical regions to identify TS. Each combination of texture feature and anatomical regions was corrected using the False-Discovery Rate (FDR), which later indicated that regions such as putamen, caudate, cingulate cortex, prefrontal, temporal, and parietal cortex had the highest correlation with defining TS patients.

Shape features are also a powerful domain where techniques are responsible to distinguish the border/shape of an object. In Yeh (Yeh, 2020), the author adopted shape analysis to diagnose brain tumors by examining the morphology of association pathways in the human brain. The study not only used structural MR images but also diffusion MR scans. However, the literature involving shape features combined with medical images is still an open subject, but it deserves attention since it has been proved that it is essential to detect changes in boundaries. As expected, no other work in our literature showed the use of shape extraction to identify TS patients.

It has been evident that using machine learning after image features (*i.e.*, texture and shape) improves the classification results. However, there is an ap-

parent limitation when those topics are implemented towards identifying TS since most of the studies are mainly performed using clinical input. We identified that the major reasons for such limitation is the lack of publicly available dataset and slight changes in the brain between TS and healthy subjects rather than the importance of image features.

This work differs from the literature due to: (1) Addressing the understanding of TS using texture and shape features; (2) Applying feature extraction aligned with a classifier in specific regions, instead of addressing the entire brain volume; and (3) Presenting a selection of region-based classifiers that are more suitable to predict TS.

### 3 MATERIALS AND METHOD

In this section, we define our materials and method used for this work (Figure 2). In essence, our method consists of four main steps: (1) *Data acquisition*, describing the dataset used; (2) *Preprocessing and Volume Parcellation*, consisting in the preprocessing steps followed by the partitioning of the brain into anatomical regions; (3) *Feature extraction*, considering texture and shape feature extraction and (4) *Classification*, involving a classifier to distinguish TS from NH subjects.

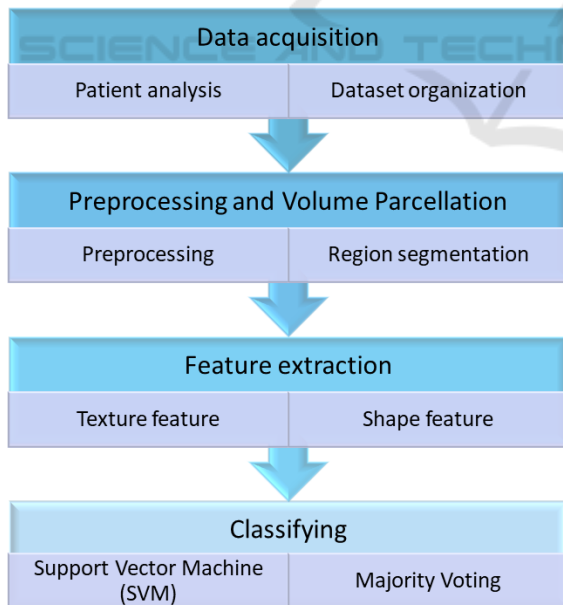


Figure 2: Proposed method to classify TS patients.

### 3.1 Data Acquisition

For data collection, all patients followed a screening process to select candidates based solely on ages between 6 to 14 years. The inclusion criteria of participants are: 1) treatment naive participants without other underlying neurological disease (*e.g.*, ADHD and OCD); 2) images without excessive head motion (artifacts) during scanning.

A total of 68 subjects were selected, organized into two equal groups (*i.e.*, 34 in each). The TS group consisted of 23 males and 11 females, aged between 6 and 13, whereas the Normal Health (H) group comprised 24 males and 10 females, aged 6 to 14. For each patient, a structural Magnetic Resonance (MR) images weighted in T1 (T1-w) were acquired using the SIEMENS Triotrim model scanner. The following MR protocols were used for the acquisition: time of echo = 2.98ms, repetition time = 2000ms, inversion time = 900ms. Each volume consisted of  $192 \times 208 \times 256$ , isotropic resolution of  $1\text{mm}^3$ , flip angle =  $9^\circ$ , and slice thickness = 1mm.

### 3.2 Preprocessing and Volume Parcellation

parcellate automatic the brain volume. We adopted Freesurfer version 6.0 to automatically segment brain volume. In general aspects, Freesurfer can be decomposed into three major steps, as described by Fischl (Fischl et al., 2002). (1) *Image preprocessing*, involving normalization, contrast enhancement, noise reduction, and registration. The preprocessed images are skull-stripped to retain only brain tissue (Figure 3.b), (2) *Brain surface inflation*, building a surface model to represent the cortical area, which is then inflated to registered to a spherical atlas. (3) *Brain segmentation*, assigning voxel-wise labels from distinct atlases. In this work, we adopted the DKT-atlas (Figure 3.c), which decomposes the cortical area into smaller groups. The regions of interest (ROI) used for our work are presented in Table 1.

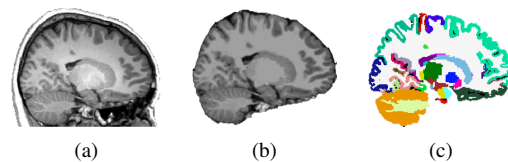


Figure 3: Preprocessing and volume segmentation for freesurfer. (a) Original image normalization; (b) skull stripping; (c) DKT-Atlas.

Table 1: Anatomical brain regions used in this work.

Deep Gray-matter	Cortical area
Thalamus (L+R)	Medial Orbitofrontal (L+R)
Caudate (L+R)	Inferior Parietal (L+R)
Putamen (L+R)	Superior Parietal (L+R)
Accumbens(L+R)	Lateral Orbitofrontal (L)
Ventral DC (L+R)	

L = left hemisphere, R = right hemisphere, DC = diencephalon.

### 3.3 Feature Extraction

Two styles of feature extraction techniques were considered to this work: (1) texture, and (2) shape. Texture and shape features are often used in controversial aspects, but we believe that important, yet complementary, information can be acquired from both of them.

**Texture Features.** The *Gray Level Co-occurrence Matrix (GLCM)* was chosen to extract texture features as it enables the analysis of the configuration of pixel transitions in a volume. This technique has been proven to provide reliable outcomes to distinguish pathological/disorder stages from normal subjects (Syed et al., 2023; Gengeç Benli and Andaç, 2023). In summary, GLCM involves the extraction of dependable texture features through the occurrence matrices (Haralick et al., 1973). The gray-scale values within the image are represented in a co-occurrence matrix as indices of a given row  $v_1$  and column  $v_2$ , and the interaction function denoted as  $f(v_1, v_2)$  signifies the count of occurrences from  $v_1$  to  $v_2$ .

The computation of pixel transitions primarily relies on two parameters: 1) the angle  $\theta$ , set to four possible directions ( $0^\circ$ ,  $45^\circ$ ,  $90^\circ$ ,  $135^\circ$ ), representing the orientation between  $v_1$  and  $v_2$  and stored in distinct GLCMs; 2) the distance  $d$ , set to 1 (adjacent correspondences), corresponding to the pixel or voxel interval between  $v_1$  and  $v_2$ . Two modifications have been introduced to the GLCM methodology: Since 3D structures are being used (26-connectivity) as opposed to 2D structures (8-connectivity), additional directions have been incorporated to calculate the displacement vector  $(dx, dy, dz)$ . The GLCM analysis has been reformulated to focus on anatomical regions rather than the entire brain, disregarding occurrences of voxels that do not belong to a specific region. In essence, each anatomical region is associated with its distinct GLCM. In conclusion, to construct the final vector encapsulating information for each region per subject, twenty-four GLCM-based metrics have been computed: Autocorrelation; Joint Average; Cluster Prominence; Cluster Shade; Cluster Tendency; Contrast; Correlation; Difference Average; Difference Entropy; Difference Variance; Joint Energy; Joint Entropy; Informational Measure of Cor-

relation 1 and 2; Inverse Difference Moment; Maximal Correlation Coefficient; Inverse Difference Moment Normalized; Inverse Difference; Inverse Difference Normalized; Inverse Variance; Maximum Probability; Sum Average; Sum Entropy; Sum of Squares (pyradiomics community, 2016).

**Shape Features.** In this work we apply *Heat Kernel Signature (HKS)* according to (Bronstein and Kokkinos, 2010a) studies and evaluate the changes in a more significant way between brain regions. HKS is a local shape analysis that uses geometric properties of forms (Bronstein and Kokkinos, 2010a). Through a multiple mesh, the application of the heat diffusion property can be represented by Equation 1.

$$\left(\Delta + \frac{\partial}{\partial t}\right)\mu(x, t) = 0 \quad (1)$$

where the negative Laplace-Beltrami operator is represented by  $\Delta$ , and the distribution and composition of heat points at a location  $x$  over time  $t$  is denoted by  $\mu(x, t)$ .

The main diagonal of the heat kernel is used as a feature descriptor in surface analyses. For each point  $x$  on the surface, an individual feature vector is computed, representing its Heat Kernel Spectrum (Sun et al., 2009). This calculation is represented by Equation 2, which describes the quantification of heat at a specific point  $x$  after a particular time period  $t$ .

$$HKS(x) = c(x)(K_{t_1}(x, x), \dots, K_{t_n}(x, x)) \quad (2)$$

where the variable  $c(x)$  satisfies the condition  $\|HKS(x)\|_2 = 1$ . The calculation of HKS is based on the analysis of the eigenvalues and the initial eigenfunctions of the Laplace-Beltrami operator.

Some limitations of HKS are related to scale sensitivity. In this work, to address this potential obstacle, we utilize the Scale-Invariant Heat Kernel Signature (SIHKS) (Bronstein and Kokkinos, 2010b), as described below.

$$h_{\text{diff}}(x) = \left( \log K_{\alpha^{\tau_2}}(x, x) - \log K_{\alpha^{\tau_1}}(x, x), \right. \\ \left. \log K_{\alpha^{\tau_m}}(x, x) - \log K_{\alpha^{\tau_{m-1}}}(x, x) \right) \quad (3)$$

$$\text{SIHKS}(x) = \|(F_{h_{\text{diff}}}(x))(\omega_1, \dots, \omega_6)\| \quad (4)$$

where the representation of the Fourier transform is given by  $F$ , and the frequency is  $\omega$ .

Figure 4 illustrates the decomposition of SIHKS.



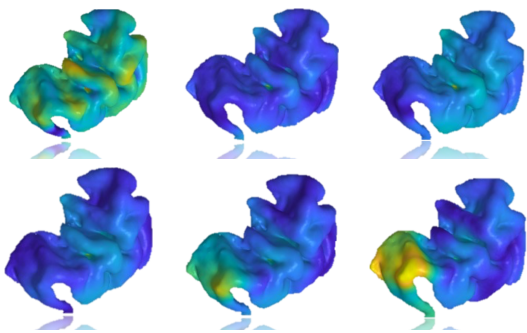


Figure 4: Distinct frequencies of SIHKS applied to the superior parietal cortex.

### 3.4 Classification and Ensemble

**Classification.** The Support Vector Machine (SVM) was chosen due to its ability to classify linearly separable data with two classes (TS and control) through the construction of hyperplanes (Feng et al., 2016). We utilized a linear kernel and set the regularization parameter  $C = 1$ , which essentially determines the configuration of the hyperplane margin. The construction of the hyperplanes can be defined as:

$$\min_{w,b} \frac{1}{2} w^T w + C \sum_{i=1} \max(0, 1 - y_i(w^T \phi(x_i) + b)) \quad (4)$$

where,  $w, b$  are hyperplane parameters;  $C$  is the regularization parameter (strictly positive), and  $x$  represents the input variables.

After proper construction and adjustment of the hyperplane, the SVM needs to distinguish between the types of samples to be analyzed, as represented by Equation 5.

$$I(x) = \text{sgn}\left(\sum_{i=1}^n u_i a_i^0(x \cdot x_i) + b\right) \quad (5)$$

To maintain the reliability of the results, we adopted the application of k-fold cross validation.

The process was divided into  $n = 68$ , representing the total number of samples in our dataset, with  $k = 10$  indicating the partition of the data. This division resulted in 8 sets with 7 samples each and 2 sets with 6 samples each, which were trained in 10 iterations.

**Majority Voting.** We adopted the ensemble via majority voting to combine the best anatomical regions (identified by accuracy of the models). This step is performed to aggregate predictions from multiple models and enhance performance. Notably, we performed the ensemble for two scenarios: texture features followed by SVM and shape features followed by SVM. The majority voting can be obtained by the following formula:

Best Regions	Classifiers' response (per subject)												#N
	#1	#2	#3	#4	#5	#6	#7	#8	#9	#10	#11	#12	
1 <sup>st</sup> Region	1	0	1	0	1	0	1	0	1	0	0	0	1
2 <sup>nd</sup> Region	0	1	0	1	0	0	1	0	0	0	1	0	1
3 <sup>rd</sup> Region	0	1	1	0	1	0	0	1	1	1	1	1	0
Outcome	0	1	1	0	1	0	1	0	1	0	1	0	1

Figure 5: Generation of a Election-based Majority voting considering the top 3 regions in accuracy. This concept can be extend to Top 5 regions. Predicting 1 means having TS, and 0 is considered as normal control.

$$R_f = \begin{cases} 1 & \text{if } \frac{\sum_{i=1}^N R_i}{N} > 0.5 \\ 0 & \text{otherwise} \end{cases} \quad (6)$$

where  $R_f$  denotes the final response,  $R_i$  is the response per region, and  $N$  is the number of regions specified by Top  $N$ .

In other words, the majority voting process selects the most frequently predicted class among the ensemble of regions. For instance, if, for each patient, across the top three regions, two indicate that the patient belongs to the TS class, and the other indicates the normal class, then the majority vote would assign the TS class as the final prediction. Our results were analyzed by assessing the responses of the top three (Top 3) and top five (Top 5) best-performing regions in this study. A more in-depth visualization of the Top 3 outcomes is shown in Figure 5.

### 3.5 Computational Tools

The implementation of this work was carried out on a macOS High Sierra version 10.13.6. with i5 processing and 16Gb of RAM. Our codes was mostly developed in Python 3.8 using the Spyder platform. Our approach was executed utilizing the subsequent tools and methodologies:

1. *Preprocessing and Volume Parcellation.* Bash scripts were created to automatically utilize the Freesurfer tool with the *recon-all* command. We separated the regions into independent volumes (for texture analysis) and meshes (for shape analysis - using ITK).
2. *Feature Extraction.* We used pyRadiomics library in Python to compute the GLCM for the volumes, whereas we adopted an independent code to compute the SIHKS in Matlab R2018a.
3. *Classifying.* The SVM was computed using the scikit-learn package, while the Majority Voting was coded from scratch.

The analyses and applications used in this study, as well as the models and figures, can be verified and

downloaded from our freely-available GitHub repository<sup>1</sup>.

## 4 RESULTS

In this study, five metrics were adopted, namely: (1) Precision, denoted as P; (2) Recall, referred as R; (3) F-score, denoted as F; (4) Accuracy, represented by A;

These metrics are derived by incorporating values such as true-positive (TP), true-negative (TN), false-positive (FP), and false-negative (FN). The calculation of these evaluation metrics is expressed by the following formulas:

$$P = \frac{TP}{TP+FP}, R = \frac{TP}{TP+FN}, F = 2 \times \frac{P \cdot R}{P+R} \quad (7)$$

$$A = \frac{TP+TN}{TP+TN+FP+FN} \quad (8)$$

Each metric was applied to evaluate both individual anatomical regions and their corresponding ensembles. We preferred ranking the regions by accuracy values, and including the top three (*Top 3*) and five (*Top 5*) best regions as part of the ensembles using Majority Voting. The best regions, along with the ensembles, are shown both for the shape- (Table 2) and texture-based classification (Table 3). In Figure 6, we show the accuracy of each anatomical region, followed by the ensembles (Top 3 and Top 5).

## 5 DISCUSSION

Tourette’s syndrome is an area that requires attention since patients around the globe suffer from involuntary movements that can directly affect their social integration. Patients who suffer from TS sometimes try to mask their tics, possibly causing discomfort and worsening the tic when released (Eapen et al.,

2016). TS is often detected clinically, but patients can mask the tic, thus generating possible false-negatives. However, implementing techniques to identify brain biomarkers for TS is a challenging task due to its supposedly modest brain changes. Thus, our primary effort in this paper is classifying TS based on image features to later enable a more in-depth understanding of brain changes.

According to Figure 6 and Table 2, notably some crucial regions achieved higher accuracy. The *right thalamus* (92.6% accuracy in shape analysis) has the role of integrating sensory (including emotional responses) and motor stimuli between the central and peripheral nervous systems. This result aligns with the current literature that highlights the thalamus as a target structure to understand TS (Baldermann et al., 2021). The *right accumbens area* (92.6% accuracy in shape analysis) plays a vital role in regulating emotional stimuli and is associated with the learning process. This region is often used to study comorbidities frequently observed in Tourette Syndrome, such as ADHD (McCairn et al., 2016; Zhu et al., 2016). Although the texture feature results have achieved lower accuracy when compared to shape feature results, it is crucial to highlight the pivotal role that understanding texture changes helps to better discriminate TS from normal control. The *right putamen* (73.5% accuracy in texture analysis) plays a role in regulating movement, initiating and modulating voluntary body actions. This region, which is located in a subcortical area forming part of the striatum, has been focused on studying TS and its patterns (Rae et al., 2019). The *thalamus* located in the left hemisphere (73.5% accuracy in texture analysis) has a vital role in relaying sensory information between the right part of the body to the cerebral cortex. This region was studied in order to characterize TS (Müller-Vahl et al., 2014).

Both classifiers (shape and texture) displayed similar behavior in achieving high accuracy of *thalamus* and the *orbitofrontal* and *prefrontal cortex*. Another relevant pattern to mention is the location of the best regions. In both techniques, the most influential regions are subcortical, more precisely part of the lim-

Table 2: Evaluation of the classification using Shape features.

#	Region Name	A	P	R	F
Individual brain regions					
1	Accumbens (R)	92.6	91.4	94.1	92.7
2	Thalamus (R)	92.6	93.9	91.1	92.5
3	Lateral orbitofrontal (L)	91.1	93.7	88.2	90.9
4	Accumbens (L)	89.7	86.4	94.1	90.1
5	Medial orbitofrontal (R)	89.7	88.5	91.1	89.8
Ensembles					
	Top 3	90.0	83.0	100.0	91.0
	Top 5	96.0	92.0	100.0	96.0

<sup>1</sup><https://github.com/hidden-for-peer-review>

Table 3: Evaluation of the classification using Texture features.

#	Region Name	A	P	R	F
Individual brain regions					
1	Putamen (R)	73.5	72.2	76.4	74.2
2	Thalamus (L)	73.5	75	70.5	72.7
3	VentralDC (R)	70.5	68.4	76.4	72.2
4	Medial orbitofrontal (R)	66.1	65.7	67.4	66.6
5	Lateral orbitofrontal (L)	66.1	67.7	61.7	64.6
Ensembles					
	Top 3	77.9	77.1	79.4	78.2
	Top 5	79.4	77.7	82.3	79.9

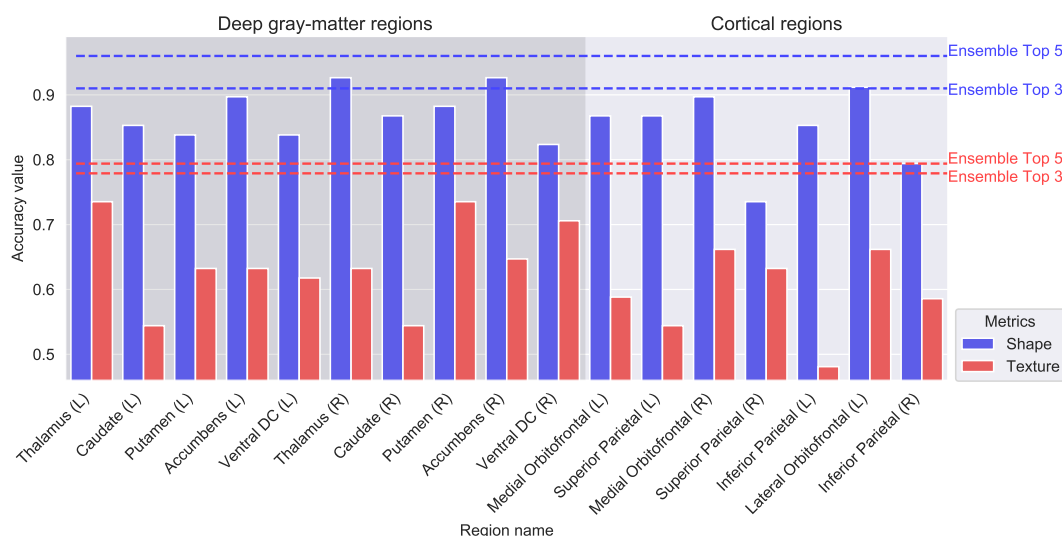


Figure 6: Accuracy values by regions, among shape features, texture, and combinations of the three and five best regions.

bic system of the brain, which are stimulated during the occurrence of tics (Leisman and Sheldon, 2022).

In order to reinforce the robustness and achieve higher accuracy of our method, we adopted ensembles, which combined the best regions in each case. When using shape features, we achieved the highest performance, reaching 96% accuracy in the Top 5, whereas we achieved 79% accuracy for the Top 5 in our texture analysis. This corroborates the effectiveness of using ensemble methods when combining distinct regions to achieve higher predictiveness. This can possibly suggest that evaluating a combination of regions instead of single regions can be a path to thrive in the better understanding of TS.

## 6 SUMMARY & CONCLUSIONS

Exploring the application of texture and shape features to evaluate anatomical brain regions in the context of TS classification represents a novel area, largely unexplored by the current state-of-the-art. Thus, we proposed a comparative analysis between two types of descriptors to discern which is more effective in predicting TS. We analyzed each individual brain region separately, as well as their combination into ensembles. We noticed that SVM demonstrated higher accuracy when using shape features, while further investigation is needed to grasp the potential of texture features.

We observed that the regions of the limbic system, more specifically the accumbens area and the thalamus, showed remarkable accuracy values in the analysis of shape features, while the putamen and the tha-

lamus presented higher accuracy in our texture analysis. The presence of the thalamus in both analyses suggests that the region plays a fundamental role in the occurrence of symptoms associated with TS. This structure is responsible for integrating sensory information and communicating with associative cortical areas. On the other hand, the orbitofrontal medial cortex has shown relevant accuracy in both descriptors, aligning with the literature since it processes emotional information, makes decisions, and regulates social behavior. The presence of these regions only reinforces the accuracy of the models presented in this work and enables further questions about the importance of other regions.

The study sheds light to some future directions: (1) the need for improved and more comprehensive descriptors to distinguish TS from NH subjects; (2) a study exploring deep learning as an automatic feature extraction method; (3) the adoption of alternative classifiers and feature descriptors.

## REFERENCES

Baldermann, J. C., Kuhn, J., Schüller, T., Kohl, S., Andrade, P., Schleyken, S., Prinz-Langenohl, R., Hellmich, M., Barbe, M., Timmermann, L., Visser-Vandewalle, V., and Huys, D. (2021). Thalamic deep brain stimulation for tourette syndrome: A naturalistic trial with brief randomized, double-blinded sham-controlled periods. *Brain Stimulation*, 14.

Barros, M. C., Duarte, K. T., Lee, W.-T., Hsu, C.-J., and de Carvalho, M. A. G. (2022). Analysis of the statistical significance of 3d texture features in mri images toward the detection of tourette’s syndrome. In

- 2022 35th SIBGRAPI Conference on Graphics, Patterns and Images (SIBGRAPI), volume 1, pages 103–108.
- Betrouni, N., Moreau, C., Rolland, A.-S., Carriere, N., Chupin, M., Kuchcinski, G., Lopes, R., Viard, R., Defebvre, L., and Devos, D. (2021). Texture-based markers from structural imaging correlate with motor handicap in parkinson's disease. *Scientific Reports*, 11:2724.
- Bronstein, M. M. and Kokkinos, I. (2010a). Scale-invariant heat kernel signatures for non-rigid shape recognition. In *2010 IEEE Computer Society Conference on Computer Vision and Pattern Recognition*, pages 1704–1711.
- Bronstein, M. M. and Kokkinos, I. (2010b). Scale-invariant heat kernel signatures for non-rigid shape recognition. In *2010 IEEE Computer Society Conference on Computer Vision and Pattern Recognition*, pages 1704–1711.
- Cen, S.-s., Yu, J., Wang, Q., Deeb, W., Wang, K.-l., Shukla, A. W., Malaty, I., Ramirez-Zamora, A., Zhang, J.-g., Hu, W., and Meng, F.-g. (2020). Multidisciplinary telemedicine care for tourette syndrome: Minireview. *Frontiers in Neurology*, 11.
- Eapen, V., Cavanna, A. E., and Robertson, M. M. (2016). Comorbidities, social impact, and quality of life in tourette syndrome. *Frontiers in psychiatry*, 7:97.
- Feng, W., Sun, J., Zhang, L., Cao, C., and Yang, Q. (2016). A support vector machine based naive bayes algorithm for spam filtering. In *2016 IEEE 35th International Performance Computing and Communications Conference (IPCCC)*, pages 1–8. IEEE.
- Fischl, B., Salat, D. H., Busa, E., Albert, M., Dieterich, M., Haselgrove, C., van der Kouwe, A., Killiany, R., Kennedy, D., Klaveness, S., Montillo, A., Makris, N., Rosen, B., and Dale, A. M. (2002). Whole brain segmentation: Automated labeling of neuroanatomical structures in the human brain. *Neuron*, 33(3):341–355.
- Gengeç Benli, Ş. and Andaç, M. (2023). Constructing the schizophrenia recognition method employing glm features from multiple brain regions and machine learning techniques. *Diagnostics*, 13(13):2140.
- Haralick, R. M., Shanmugam, K., et al. (1973). Textural features for image classification. *IEEE Transactions on systems, man, and cybernetics*, 6:610–621.
- Johnson, K. A., Worbe, Y., Foote, K. D., Butson, C. R., Gunduz, A., and Okun, M. S. (2023). Tourette syndrome: clinical features, pathophysiology, and treatment. *The Lancet Neurology*, 22(2):147–158.
- Jones, K. S., Saylam, E., and Ramphul, K. (2023). Tourette syndrome and other tic disorders. *StatPearls*.
- Kamarajugadda, K. K. and Pavani, M. (2022). Multi-features assisted age invariant face recognition and retrieval using cnn with scale invariant heat kernel signature. In Fernandez, M. A. A. and Travieso-Gonzalez, C. M., editors, *Artificial Intelligence Annual Volume 2022*, chapter 8. IntechOpen, Rijeka.
- Leisman, G. and Sheldon, D. (2022). Tics and emotions. *Brain Sciences*, 12(2).
- McCairn, K., Nagai, Y., Hori, Y., Ninomiya, T., Kikuchi, E., Lee, J.-Y., Suhara, T., Iriki, A., Minamimoto, T., Takada, M., Isoda, M., and Matsumoto, M. (2016). A primary role for nucleus accumbens and related limbic network in vocal tics. *Neuron*, 89(2):300–307.
- Müller-Vahl, K. R., Grosskreutz, J., Prell, T., Kaufmann, J., Bodammer, N., and Peschel, T. (2014). Tics are caused by alterations in prefrontal areas, thalamus and putamen, while changes in the cingulate gyrus reflect secondary compensatory mechanisms. *BMC Neuroscience*, 15(1).
- Pringsheim, T., Ganos, C., Nilles, C., Cavanna, A. E., Gilbert, D. L., Greenberg, E., Hartmann, A., Hedderly, T., Heyman, I., Liang, H., Malaty, I., Malik, O., Debes, N. M., Vahl, K. M., Munchau, A., Murphy, T., Nagy, P., Owen, T., Rizzo, R., Skov, L., Stern, J., Szejko, N., Worbe, Y., and Martino, D. (2023). European society for the study of tourette syndrome 2022 criteria for clinical diagnosis of functional tic-like behaviours: International consensus from experts in tic disorders. *European Journal of Neurology*, 30(4):902–910.
- pyradiomics community (2016). Radiomic features.
- Rae, C. L., Critchley, H. D., and Seth, A. K. (2019). A bayesian account of the sensory-motor interactions underlying symptoms of tourette syndrome. *Frontiers in Psychiatry*, 10.
- Silva, J., Bispo, B., and Rodrigues, P. (2023). Structural mri texture analysis for detecting alzheimer's disease. *Journal of Medical and Biological Engineering*.
- Sun, J., Ovsjanikov, M., and Guibas, L. (2009). A concise and provably informative multi-scale signature based on heat diffusion. *Computer Graphics Forum*, 28(5):1383–1392.
- Syed, A., Adam, R., Ren, T., Lu, J., Maldjian, T., and Duong, T. Q. (2023). Machine learning with textural analysis of longitudinal multiparametric mri and molecular subtypes accurately predicts pathologic complete response in patients with invasive breast cancer. *PloS one*, 18(1):e0280320.
- Tourette.org, o. (2017). Iceberg illustration poster.
- Yeh, F.-C. (2020). Shape analysis of the human association pathways. *NeuroImage*, 223:117329.
- Zhu, Y., Yang, D., Ji, W., Huang, T., Xue, L., Jiang, X., Chen, L., and Wang, F. (2016). The relationship between neurocircuitry dysfunctions and attention deficit hyperactivity disorder: A review. *BioMed Research International*, 2016:1–7.